Evaluation of SAR-Optical Imagery Synthesis Techniques in a Complex Coastal Ecosystem

Floyd M. Henderson, Robert Chasan, Jamie Portolese, and Thomas Hart, Jr.

Abstract

Coastal areas comprise some of the world's most important and sensitive ecosystems. Although optical remote sensing systems have demonstrated an ability to map land cover in many coastal environments, spectral confusion has also been reported. The parameters of SAR imagery suggest that combinations of SAR and optical data may improve land-cover classification accuracy. Seven satellite SAR data sets were merged with TM data using four techniques. These were tested by classifying 11 upland and wetland land covers in a rapidly urbanizing coastal area of the northeast United States. Not all SAR/TM combinations bettered the accuracy obtained using TM data alone. In general, simple techniques improved accuracy more than did complex image merge methods. Although one SAR image proved superior overall, improvement in detection accuracy varied among individual land-cover categories and SAR data. The results point to the possible benefits of hierarchical/layered classifications.

Introduction

Coastal areas comprise some of this planet's most complex and productive ecosystems (Mitsch and Gosselink, 1993). Around 60 percent of the world's total population lives in the narrow coastal strip between sea level and 200 m above sea level (Cracknell, 1999). Focal points for human culture, these areas have historically been among the world's most dynamic environments. As human population networks expand inland, large natural area tracts are sub-divided and developed. The result is a complex ecosystem in transition—a fragmented landscape consisting of a mixture of natural and cultural land cover. For proper environmental management of these areas, land-cover information that can be obtained and updated in a timely manner is critical.

Numerous investigations have shown that optical remote sensing systems can be used to classify and map land cover in coastal environments (Jensen *et al.*, 1993; Henderson *et al.*, 1999). However, spectral signature confusion among optical-sensor-based land-cover categories has been reported along with degraded classification accuracy. For example, parking lots, sandy beaches, building surfaces, and tilled fields often appear spectrally similar as do some forested and forested wetland areas (Kershaw and Fuller, 1992; Henderson *et al.*, 1999).

Satellite-based synthetic aperture radar (SAR) systems have recently shown potential for identifying land-cover types as well as particular land-cover conditions (Dobson *et al.*, 1995a; Dobson *et al.*, 1996; Schmullius and Evans, 1997). The bio- and geo-physical parameters of SAR suggest that active microwave sensors contribute electrical and morphological information that, used in concert with optical sensors, may reduce optical classification confusion among urban and non-urban land covers (Taket *et al.*, 1991; Dong *et al.*, 1997; Henderson and Xia, 1998).

Efforts to combine optical and SAR imagery have been reported. Pohl and Van Genderen (1998) provide an extensive review of image fusion concepts, methods, and applications based on some 169 articles. Included among the potential benefits discussed were image sharpening, increased temporal and/or spatial resolution, improved registration accuracy, feature enhancement, and improved classification. Yet within this body of research relatively few works have focused on SAR imagery of urban and rapidly urbanizing coastal areas.

C-band SAR data, especially HH-polarized imagery, have been reported as effective in delineating herbaceous and forested wetlands from other land-cover types in rural areas (Kasischke *et al.*, 1997; Wang *et al.*, 1998; Murphy *et al.*, 2001; Baghdadi *et al.*, 2001). Toll (1985) reported the benefits of combining SAR and Landsat MSS data to map urban land cover in Denver, Colorado. Dong *et al.* (1997) and Henderson and Xia (1998) have analyzed the attributes of SAR that suggest it would be useful in urban monitoring. A search of the literature indicates that no work has concentrated specifically on urban coastal areas to report on the merits of merging optical/SAR data in such environments.

This paper presents the results of digital image land-cover classifications in a complex, rapidly urbanizing coastal ecosystem using combinations of satellite-based SAR and Landsat Thematic Mapper (TM) images. The purpose was to quantitatively evaluate SAR/optical image merge techniques that use the spectral and in some cases spatial resolution contributions of SAR data in defining wetland and upland land-cover types in urban coastal regions. The study gives particular attention to

F.M. Henderson is with the GIS and Remote Sensing Laboratory, Department of Geography and Planning, University at Albany, The State University of New York, Albany, NY 12222 (f.henderson@albany.edu).

R. Chasan is with the City of Scottsdale GIS, 3629 N. Drinkwater Blvd., Scottsdale, AZ 85251 (rchasan@ci.scottsdale.az.us).

J. Portolese is with Viewpoint Engineering, 500 West Commings Park, Woburn, MA 01801.

T. Hart, Jr., is with the New York State Department of Health, Albany, NY 12203.

Photogrammetric Engineering & Remote Sensing
Vol. 68, No. 8, August 2002, pp. 839–846.

0099-1112/02/6808–839$3.00/0

the contribution of C-band SAR data to resolving optical spectral confusion between wetlands and non-wetlands and between urban and non-urban land covers.

Study Area and Methodology

The Carmans-Forge Rivers region of Long Island, New York served as the focus of this study (72.88°W; 40.77°N) (Figure 1). The area is typical of many American coastal areas at the confluence of urban sprawl and natural/agricultural open spaces. The 172-sq-km area contains a mix of rural and urban land cover as well as one of the island's major drainage systems. Open and natural areas include woods, bare ground, wetlands, pastures, grasslands, and cultivated fields. These natural areas are intermixed with urban development and impervious surfaces in a collage of heterogeneous land cover. Between 1940 and 1990 population in this area increased 570 percent; between 1980 and 1990 housing units increased 11 percent (Chasan, 1998).

The National Oceanic and Atmospheric Administration (NOAA) Coastal Change Analysis Program (C-CAP) has developed a protocol and classification system for mapping coastal wetlands and adjacent upland land cover for any coastal region in the United States based primarily on analysis of Landsat TM data (Dobson *et al.*, 1995b). The eleven land-cover categories used in this investigation followed C-CAP protocol recommendations. They included the four wetland classifications present in the study area (Estuarine Emergent; Palustrine Emergent; Palustrine Scrub Shrub; Palustrine Forested), six upland cover types (Bare Ground; Grasslands/Cultivated; Deciduous Forest; Coniferous Forest; Impervious Surfaces; Developed) and Water. A brief description of their composition is provided in Table 1.

Imagery

A list of the original image data sets and their characteristics are shown in Table 2. In addition, two artificial SAR images were created from Principal Components Analysis (PCA) of multiple SAR scenes. The intent was to retain the common information found in the multiple SAR scenes while reducing the dimensionality of the data sets to be combined with the TM data. The first artificial SAR image combined the F2N and F4N Radarsat fine mode images to consider the potential benefit of information contained in high-resolution, multi-date SAR images; the second used three Radarsat Standard Mode images (S1, S2A, S7) to evaluate the contribution of multiple incident angle data of moderate spatial resolution. In each case the first principal component of the SAR image suite (PC1) was selected for merger with the TM data.

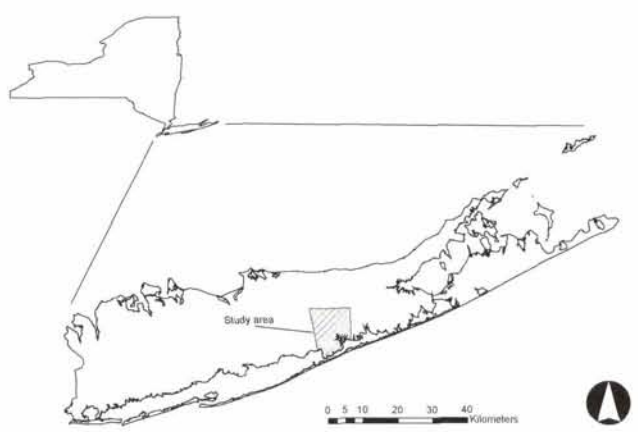

Figure 1. Study Area.

TABLE 1. LAND-COVER CATEGORIES AND THEIR CHARACTERISTICS

Category	Principal Species and/or Characteristics
Water	Ocean, bays, rivers, creeks, lakes, ponds
Estuarine Emergent	*Spartina alterniflora, Spartina patens* Tidal saltwater marshlands
Palustrine Emergent	*Phragmites australis* Non-tidal permanent wetlands of inland freshwater marshes
Palustrine Forest	*Acer rubrum, Chamaecypars thyoids* Non-tidal freshland wetlands with > 50% tree canopy cover
Palustrine Scrub Shrub	*Pinus rigida, Quercus var, Chaemaeadaphnae calyculata* Transition zone between coastal freshwater wetlands and pine-oak barrens
Bare Ground	Undeveloped with little or no vegetation. Includes shoreline, landfills, non-cultivated tilled farmland
Coniferous Forest	*Pinus spp.* Contiguous stands of needle-leaf evergreen trees
Deciduous Forest	*Quercus spp., Acer spp.* Contiguous stands of broad-leafed trees
Grass/Cultivated	Managed and unmanaged grasslands, cultivated farm land, golf courses, cemeteries, large lawns, recreational fields
Developed	Mixed class composed of suburban development. Includes structures, lawns, streets. Imperviousness < 80%
Impervious	Imperviousness > 80%. Includes parking lots, major roadways, commercial and industrial landuse

All scenes were co-registered to an existing database that had previously been rectified and registered using ground control points gathered with differentially corrected Global Positioning System data. The SAR images were registered using cubic convolution resampling; the TM image was registered using nearest-neighbor resampling (Heaton, 1998). A 9 by 9 Lee filter was applied to each of the SAR data sets to reduce image speckle (Durand *et al.*, 1987; Lee *et al.*, 1994; Chasan, 1998).

Image Combination Techniques

Two different approaches were used to digitally combine data sets: (1) synthesis and (2) concatenation. For compatibility and consistency among merged sets of different spatial resolutions, the data set with the coarsest spatial resolution was always resampled to the data set having the higher spatial resolution. In all, four image combination methods were tested.

Synthetic mergers mathematically join all pixel values to create synthetic pixel values. Three synthetic methods were tested. Two of these methods employ the addition of SAR to TM pixel values in selected bands. They were based on the success of previous research in visually delineating coastal features in Louisiana (Lewis *et al.*, 1995). The third synthetic technique, commonly referred to as image fusion, involves Principal Component Analysis (PCA) and Inverse Principal Component Analysis of the data sets. Here, the pixel values of a second data set are substituted for one of the principal components of the first data set and an Inverse PCA is performed. In this method, the values of the second data set are "fused" or distributed throughout the remaining bands of the first data set.

The concatenation merge technique simply adds a single-channel data set to a multi-channel data set as an additional

TABLE 2. ORIGINAL IMAGE DATA AND THEIR CHARACTERISTICS

Type	Look Direction	Incident Angle	Pixel Size	Polarization	Acquisition Date
Radarsat F2N	Ascending	40.3	6.25m	HH	16 Apr 97
Radarsat F4N	Ascending	44.6	6.25m	HH	08 May 97
Radarsat S7	Ascending	46.9	24m	HH	20 May 97
Radarsat S2A	Ascending	27.5	24m	HH	24 May 97
Radarsat S2D	Descending	27.5	24m	HH	28 May 97
Radarsat S1	Ascending	23.1	24m	HH	24 Jun 97
ERS-1	Ascending	23	30m	VV	25 May 96
Landsat TM (bands 1–5 & 7)	—	—	25m	—	27 May 97

"band." In this case, the SAR data were concatenated to the TM data. Both the PCA fusion and concatenation techniques have been reported to have potential in SAR/optical merges (Chavez *et al.*, 1991; Lozano-Garcia and Hoffer, 1993; Pohl and Van Genderen, 1998).

A brief explanation of each of the four data merge methods follows:

Image Addition

Using TM bands 3, 5, and 7, each SAR pixel value was added to the corresponding TM band 5 and 7 pixel values, respectively (Lewis *et al.*, 1995) (Equation 1). The result was a three-band, 16-bit image: i.e.,

$$C_o = T_i + R_i \tag{1}$$

where C_o is the combined output pixel value, T_i is the input TM pixel value, and R_i is the input radar pixel value.

Weighted Addition—A Variation on Image Addition

Each SAR pixel value was added to the corresponding TM bands 3 and 5 pixel value after each of the TM bands was increased by a common multiple (Equation 2). The common multiple employed was 2 (Lewis *et al.*, 1995). The result was a three-band, 16-bit image: i.e.,

$$C_o = nT_i + R_i \tag{2}$$

where C_o is the combined output pixel value, T_i is the input TM pixel value, n is the common multiplier, and R_i is the input radar pixel value.

PCA Fusion

A Principal Components Analysis was performed on TM bands 1 through 5 and 7. The resultant data set contained six Principal Components bands. The SAR data set was then substituted for one of the principal components (e.g., PC1). An Inverse Principal Components Analysis was then performed to integrate the SAR data with the remaining TM data.

Concatenation

The Concatenation method added the SAR image as a discrete layer to the existing TM layer set. Due to the different radiometric scales of SAR and TM digital numbers (SAR 16-bit, TM 8-bit), the TM data were proportionately rescaled to 16-bit. This prevented the SAR pixel values from potentially overwhelming the TM values while retaining the original precision of the SAR data (Equation 3). The SAR image was then concatenated with the new, standardized TM image: i.e.,

$$T_n = \frac{T_i R_{MAX}}{T_{MAX}} \tag{3}$$

where T_n is the output TM pixel value, T_i is the raw input TM pixel value, T_{MAX} is the maximum possible TM pixel value (255), and R_{MAX} is the maximum 16-bit pixel value (65535).

Principal Components Analysis produces components with an arbitrary scale of values in signed floating point format with a range, from negative to positive, that may exceed 256 integer values. For consistency with the other datasets, all PC data were rescaled to 16-bit data format (Equation 4): i.e.,

$$P_n = (P_i - P_{MIN}) * \frac{R_{MAX}}{P_{MAX} - P_{MIN}} \tag{4}$$

where P_n is the output PC pixel value, R_{MAX} is the maximum possible 16-bit pixel value (65535), P_{MAX} is the highest PC pixel value, P_{MIN} is the lowest PC pixel value, and P_i is the input PC pixel value.

Imagery Combinations

The steps described above were used to create ten Image Concatenations, nine Image Additions, four Image Weightings, and five PCA Fusion data sets for analysis—a total of 28 image combinations. The combination names and their abbreviations used in the text are shown in Table 3. A brief description of the selection process follows.

Concatenation

Ten SAR/TM concatenations were evaluated. The first nine were created from all the original SAR and PC SAR data sets. The tenth was selected from the PCA Fusion substitution approaches discussed below.

Image Addition

The first nine concatenation combinations were examined using the Image Addition Method.

Image Weighting

The outcomes of the Concatenation and Image Addition classifications led to the testing of four Image Weighting combinations: the data sets that yielded the three highest Image Addition overall accuracy results plus the ERS combination for SAR polarization comparison purposes.

PCA Fusion

Earlier work evaluating the seven individual SAR data sets found that the Radarsat F2N image produced the highest overall accuracy (Henderson *et al.*, 1998). Based on that performance, the Radarsat F2N image was selected for PCA fusion with the TM 1 through 5 and 7 image. The first fusion substituted the F2N image for TM PC1 as is the normal procedure. In effect, the high spatial resolution SAR data values replaced the intensity values of the TM data. However, visual examination of the combined image set on the computer monitor and the corresponding classification accuracy results suggested that the SAR data might be overpowering the optical data. Consequently,

TABLE 3. DATA SET COMBINATIONS

Technique	Abbreviation
CONCATENATION	
TM1-5&7 with Radarsat F2N	c:F2N
TM1-5&7 with Radarsat F4N	c:F4N
TM1-5&7 with Radarsat S1	c:S1
TM1-5&7 with Radarsat S2 Ascending Pass	c:S2A
TM1-5&7 with Radarsat S2 Descending Pass	c:S2D
TM1-5&7 with Radarsat S7	c:S7
TM1-5&7 with ERS-1	c:ERS
TM1-5&7 with PC1 of F2N, F4N PCA	$c:PC_F$
TM1-5&7 with PC1 of S1, S2A, S7 PCA	$c:PC_S$
TM PC1,2,3 with Radarsat F2N	$c:TM_{PC123}+F2N$
IMAGE ADDITION	
Radarsat F2N	a:F2N
Radarsat F4N	a:F4N
Radarsat S1	a:S1
Radarsat S2 Ascending Pass	a:S2A
Radarsat S2 Descending Pass	a:S2D
Radarsat S7	a:S7
ERS-1	a:ERS
PC1 of F2N, F4N PCA	$a:PC_F$
PC1 of S1, S2A, S7 PCA	$a:PC_S$
IMAGE WEIGHTING	
Radarsat F2N	w:F2N
Radarsat F4N	w:F4N
PC1 of F2N, F4N PCA	$w:PC_F$
ERS-1	w:ERS
PCA FUSION	
TM PC2-5&7 with Radarsat F2N replacing TM PC1	$f:TM_{PC23457}+F2N$
TM PC2-5&7 with Radarsat F4N replacing TM PC1	$f:TM_{PC23457}+F4N$
TM PC1-5&7 with PC1 of F2N, F4N PCA replacing TM PC1	$f:TM_{PC23457}+PCF$
TM PC1-5&7 with Radarsat F2N replacing TM PC4	$f:TM_{PC12357}+F2N$
TM PC1,2,3 with Radarsat F2N replacing TM PC4	$f:TM_{PC123}+F2N$

it was felt that much of the spectral intensity information of the TM image might have been lost. That observation led to two additional fusion combinations.

The first of these substituted the SAR pixel values for TM PC4 instead of TM PC1. The intent was to retain the majority of optical spectral contribution of the TM scene while fusing the SAR contribution in a less dominant manner. The second approach used only the first three principal components from the TM PC data set and used the SAR data to substitute as the fourth band into the inverse PCA. TM PC4, TM PC5, and TM PC6 were dropped on the premise that they were contributing little information and the deletion of these components would reduce the dimensionality of the data set. The Radarsat F4N image was included to provide a comparison with the F2N results and with the PCA of the F2N/F4N SAR suite.

Following creation of the merged data sets, a maximum-likelihood classification was conducted on each combination. A total of 93 training sets were used to define the land cover categories. Training set selection was based on an examination of 1994 United States Geological Survey (USGS) National Aerial Photography Program (NAPP) photography (hardcopy and digital orthophoto quads), 1994 digital National Wetland Inventory data, and field work in the study area to validate land-cover conditions contemporary with TM/SAR data acquisition dates.

Accuracy Assessment

All classified output data sets were subjected to a common accuracy assessment procedure. A total of 935 accuracy points were selected by examination of digital ortho quads derived from NAPP imagery and confirmed by contemporary ground verification. These accuracy points were used to produce a confusion matrix (contingency table) for each data set. Overall Accuracy figures and Kappa Coefficients were generated (Table 4) along with Producer's Accuracy (PA) and User's Accuracy (UA) figures.

The Kappa Coefficient described how well the classification performed in comparison to a random correlation and is independent of imagery, sampling types, and classification schemes (Kalkhan *et al.*, 1997). Kappa values can range from 0 (random) to 1 (completely non-random). Monserud and Leemans (1992) assigned the following qualitative values to the Kappa statistics as interpretive aids: less than 0.4 are poor to fair; values from 0.4 to 0.75 are fair to very good; and values greater than 0.75 are considered very good to excellent. The Z-test for normal distributions was used to detect significant differences between classified image pairs for the Kappa Coefficients (Sharma and Sarkar, 1998). Table 5 shows the comparison of statistical significance among the output datasets.

PA and UA provide information on omission and commission errors. However, as these measures do not reflect the same information it is often difficult to relate the quality of a classification procedure within and among data sets. Instead, a Combined Accuracy (CA) figure, the product PA*UA, was created to allow comparison among entire data sets as well as individual land-cover categories within data sets (Table 6). The CA figure gives a measure of the land cover's classification quality relative to all other land-cover classes in all other images and, of no less importance, provides a simple measure of the utility of the data set/technique for the user (Chasan, 1998).

Analysis and Results

For comparison purposes it should be remembered that the overall accuracy for the TM1 through 5 and 7 data set alone was 79.3 percent.

TABLE 4. OVERALL ACCURACY AND KAPPA COEFFICIENTS

Technique	Accuracy	Kappa
TM 1-5 & 7 (for reference)	79.30%	0.768527
CONCATENATION		
c:F2N	**82.4%**	0.802969
c:F4N	81.3%	0.779119
c:S1	78.6%	0.761212
c:S2A	79.9%	0.775559
c:S2D	77.9%	0.753094
c:S7	78.8%	0.763625
c:ERS	80.6%	0.783821
$c:PC_F$	**82.4%**	0.803015
$c:PC_S$	80.2%	0.779146
$c:TM_{PC123}+F2N$	**82.4%**	0.803676
IMAGE ADDITION		
a:F2N	72.0%	0.690113
a:F4N	68.4%	0.650709
a:S1	61.7%	0.575245
a:S2A	65.2%	0.61456
a:S2D	64.2%	0.603111
a:S7	63.1%	0.590791
a:ERS	60.7%	0.56426
$a:PC_F$	72.0%	0.689245
$a:PC_S$	65.3%	0.615848
IMAGE WEIGHTING		
w:F2N	70.1%	0.668679
w:F4N	66.7%	0.631699
$w:PC_F$	69.6%	0.662804
w:ERS	59.7%	0.553094
FUSION		
$f:TM_{PC23457}+F2N$	80.5%	0.78301
$f:TM_{PC23457}+F4N$	77.5%	0.749681
$f:TM_{PC23457}+PCF$	80.4%	0.781797
$f:TM_{PC12357}+F2N$	81.9%	0.79834
$f:TM_{PC123}+F2N$	81.1%	0.789322

Bold indicates best results

TABLE 5. COMPARISON OF STATISTICAL SIGNIFICANCE AMONG OUTPUT DATA SETS

	TM 1-5 & 7	c:F2N	c:F4N	c:S1	c:S2A	c:S2D	c:S7	c:ERS	c:PCF	c:PCS	c:TMPC123+F2N	a:F2N	a:F4N	a:S1	a:S2A	a:S2D	a:S7	a:ERS	a:PCF	a:PCS	w:F2N	w:F4N	w:PCF	w:ERS	f:TM PC123457+F2N	f:TM PC123457+F4N	f:TM PC123457+PCF	f:TM PC12357+F2N
c:F2N																												
c:F4N																												
c:S1		Y																										
c:S2A																												
c:S2D		Y																										
c:S7		Y																										
c:ERS																												
c:PCF	Y			Y		Y	Y																					
c:PCS																												
c:TMPC123+F2N	Y			Y		Y	Y																					
a:F2N	Y	Y	Y	Y	Y	Y	Y	Y	Y	Y	Y																	
a:F4N	Y	Y	Y	Y	Y	Y	Y	Y	Y	Y	Y	Y																
a:S1	Y	Y	Y	Y	Y	Y	Y	Y	Y	Y	Y	Y	Y															
a:S2A	Y	Y	Y	Y	Y	Y	Y	Y	Y	Y	Y	Y																
a:S2D	Y	Y	Y	Y	Y	Y	Y	Y	Y	Y	Y	Y	Y															
a:S7	Y	Y	Y	Y	Y	Y	Y	Y	Y	Y	Y	Y	Y															
a:ERS	Y	Y	Y	Y	Y	Y	Y	Y	Y	Y	Y	Y	Y		Y													
a:PCF	Y	Y	Y	Y	Y	Y	Y	Y	Y	Y	Y			Y	Y	Y	Y	Y										
a:PCS	Y	Y	Y	Y	Y	Y	Y	Y	Y	Y	Y	Y						Y	Y									
W:F2N	Y	Y	Y	Y	Y	Y	Y	Y	Y	Y	Y			Y	Y	Y	Y	Y		Y								
W:F4N	Y	Y	Y	Y	Y	Y	Y	Y	Y	Y	Y	Y		Y			Y	Y	Y									
W:PCF	Y	Y	Y	Y	Y	Y	Y	Y	Y	Y	Y			Y	Y	Y	Y	Y		Y								
W:ERS	Y	Y	Y	Y	Y	Y	Y	Y	Y	Y	Y	Y	Y		Y	Y			Y	Y	Y	Y	Y					
f:TM PC123457+F2N												Y	Y	Y	Y	Y	Y	Y	Y	Y	Y	Y	Y	Y				
f:TM PC123457+F4N		Y							Y		Y	Y	Y	Y	Y	Y	Y	Y	Y	Y	Y	Y	Y	Y				
f:TM PC123457+PCF												Y	Y	Y	Y	Y	Y	Y	Y	Y	Y	Y	Y	Y				
f:TM PC12357+F2N				Y		Y	Y					Y	Y	Y	Y	Y	Y	Y	Y	Y	Y	Y	Y	Y		Y		
f:TM PC123+F2N						Y						Y	Y	Y	Y	Y	Y	Y	Y	Y	Y	Y	Y	Y		Y		

Y = Statistically Significant Difference at 95% Confidence Level.

TABLE 6. COMBINED ACCURACY PERCENTAGE FOR ALL DATA SETS/LAND-COVER CLASSES

	Bare	Conifer	Est Emg	Grass	Pal Emg	Pal For	Imperv	Pal SS	Devel	Water	Decid
TM1-5&7	88.4%	73.7%	57.9%	72.3%	7.2%	31.2%	54.7%	3.3%	60.1%	89.6%	82.4%
c:F2N	86.4%	83.8%	55.0%	77.1%	0.0%	**41.6%**	59.2%	2.6%	78.8%	92.2%	87.2%
c:F4N	84.6%	79.1%	58.3%	76.7%	0.0%	30.2%	47.6%	1.6%	73.5%	88.6%	88.3%
c:S1	83.6%	66.9%	53.9%	76.4%	0.0%	27.9%	48.0%	2.0%	74.0%	90.5%	84.3%
c:S2A	**88.5%**	72.3%	57.7%	76.2%	0.0%	25.5%	55.4%	0.7%	72.6%	92.3%	86.2%
c:S2D	86.5%	71.1%	52.1%	**80.4%**	0.0%	25.9%	49.3%	0.4%	73.0%	82.0%	85.5%
c:S7	81.8%	74.7%	51.3%	77.4%	0.0%	34.6%	44.2%	2.1%	68.1%	95.1%	84.2%
c:ERS	84.5%	75.4%	53.8%	76.0%	0.0%	36.8%	52.4%	12.9%	72.9%	86.5%	89.2%
c:PC_F	85.5%	83.2%	56.6%	77.9%	0.0%	35.7%	55.9%	4.2%	**81.3%**	92.3%	**89.4%**
c:PC_S	86.4%	81.8%	54.9%	77.4%	0.0%	30.6%	54.7%	0.2%	72.3%	**96.0%**	82.4%
c:TM_{PC123}+F2N	70.3%	**88.1%**	58.7%	80.3%	3.6%	32.7%	**71.3%**	**19.2%**	80.3%	95.0%	81.4%
a:F2N	74.1%	43.3%	20.3%	76.4%	5.1%	31.7%	58.7%	7.9%	70.1%	96.0%	72.3%
a:F4N	81.3%	43.2%	43.6%	40.5%	**7.0%**	14.3%	57.6%	6.6%	58.6%	92.2%	58.3%
a:S1	84.3%	25.6%	16.3%	46.9%	6.1%	8.7%	59.8%	0.3%	42.7%	91.3%	44.8%
a:S2A	80.4%	40.5%	17.5%	51.9%	4.1%	17.7%	54.4%	2.3%	53.5%	95.1%	50.2%
a:S2D	87.3%	32.9%	12.2%	40.3%	6.7%	21.3%	53.4%	5.7%	49.5%	97.0%	44.1%
a:S7	71.1%	29.3%	15.1%	41.3%	3.4%	17.3%	53.6%	6.2%	59.2%	96.0%	43.8%
a:ERS	82.0%	34.5%	13.0%	37.5%	1.6%	8.3%	59.8%	3.1%	41.8%	78.5%	41.0%
a:PC_F	82.4%	55.1%	28.0%	54.0%	6.3%	21.2%	52.2%	7.2%	63.7%	96.0%	73.5%
a:PC_S	75.6%	33.8%	24.5%	40.8%	1.6%	17.6%	59.2%	2.4%	60.3%	96.0%	54.4%
w:F2N	66.6%	52.2%	28.2%	68.8%	5.4%	27.8%	47.6%	5.1%	53.6%	95.0%	75.7%
w:F4N	67.6%	48.3%	40.4%	41.1%	3.7%	15.3%	49.3%	7.8%	46.9%	91.5%	61.2%
w:PC_F	79.4%	60.0%	25.8%	41.8%	1.9%	16.9%	46.7%	10.6%	58.7%	93.2%	69.3%
w:ERS	66.5%	49.9%	10.6%	31.8%	1.6%	12.3%	48.9%	1.0%	38.0%	79.4%	49.6%
f:$TM_{PC23457}$+F2N	80.3%	77.4%	**68.1%**	76.4%	4.0%	36.4%	58.7%	3.2%	60.8%	95.2%	79.2%
f:$TM_{PC23457}$+F4N	82.4%	78.6%	60.6%	68.3%	0.6%	20.3%	52.9%	2.4%	54.6%	92.2%	83.5%
f:$TM_{PC23457}$+PC_F	81.4%	79.1%	62.7%	72.4%	3.3%	29.0%	61.0%	6.4%	65.8%	92.2%	81.0%
f:$TM_{PC12357}$+F2N	82.1%	85.4%	52.6%	81.6%	2.7%	36.2%	62.8%	3.5%	78.8%	93.2%	86.1%
f:TM_{PC123}+F2N	71.4%	87.3%	58.7%	77.2%	0.0%	33.9%	62.1%	12.7%	81.1%	94.1%	79.4%

Best accuracy per land-cover class indicated in bold.

Overall Accuracy

Image Addition and Image Weighting did not produce overall accuracy figures or Kappa Coefficients as high as the PCA Fusion or Concatenation techniques (Table 4). Applying the qualitative Kappa ranking criteria described above, the TM image, all Image Concatenations and the Image Fusion data sets ranked highest, from very good to excellent. All Image Weighting and Image Addition combinations ranked slightly lower, ranging from fair to very good. We believe there may be two reasons for these groupings. The first is that the earlier success with these latter two techniques was based on visual rather than digital analysis. The human eye is a great integrator

of patterns, tones, texture, shapes, sizes, and location—abilities not yet readily available in most digital image analysis procedures. The second reason for the difference may be attributable to environmental modulation—features that can be identified in one environment and ecosystem are not always equally identifiable in another. Certainly, the rural wetland environment of coastal Louisiana is markedly different in many ways from that found on New York's Long Island. The highest overall accuracy attained by the Image Addition technique (72.0 percent) was achieved by both *a*:F2N and a:PC_F. The F2N image also produced the best overall accuracy by Image Weighting—*w*:F2N (70.1 percent).

Image Fusion by PCA proved more accurate than the other two synthetic techniques, but less accurate overall than the corresponding Image Concatenation data sets. The f:$TM_{PC12357}$ + F2N resulted in minor overall accuracy improvements versus the original substitution of f:$TM_{PC23457}$ + F2N (81.9 percent vs. 80.5 percent). The f:TM_{PC123} + F2N fell into the middle (81.1 percent).

The highest overall accuracy, 82.4 percent, was achieved by three techniques: *c*:F2N, c:PC_F, and c:TM_{PC123} + F2N. These results suggest that the computationally intensive principal components technique offered no benefit compared to the simple concatenation method. The results also suggest that Fine Mode SAR's higher spatial resolution and sensitivity to surface roughness and volume scatter were contributing factors to the overall accuracy (Table 5).

Each SAR Image Concatenation was superior to its corresponding Image Addition counterpart, reinforcing the benefit of the simple approach with regard to SAR/optical image combination. The *c*:ERS (80.6 percent) performed slightly better overall than *c*:S1 (78.6 percent) with a similar incident angle. This is apparently attributable largely to ERS' comparative stronger ability to identify Coniferous Forest because *c*:S1 proved comparatively more accurate in detecting Grasslands while Water and all other cover-type accuracies were similar. Among the Radarsat image data sets, incident angle proved less important than increased spatial resolution in improving overall accuracy.

Combined Accuracy by Land-Cover Type

The next step was to determine if the trends and results observed for overall accuracy were associated with or similar for each land-cover type. An examination of the accuracy of the different merge techniques for each land-cover category disclosed considerable variation among the different combinations (Table 6). Among the findings were that Image Weighting failed to produce the highest detection accuracy for any land cover category. One Image Fusion technique, f:$TM_{PC23457}$ + F2N, resulted in a 68.1 percent combined accuracy for the detection of Estuarine Emergent Wetland, the highest for that category. Image Addition also generated the highest combined accuracy for one land-cover type. The *a*:F4N detected the most Palustrine Emergent Wetlands (but only 7.0 percent).

Image Concatenation produced the highest combined accuracies for the other nine land-cover categories, but the specific SAR/TM combination varied among the land-cover types. Some variation of an F2N Concatenation data set was successful for six cover types: Coniferous Forest (88.1 percent), Palustrine Forest Wetland (41.6 percent), Impervious Surfaces (71.3 percent), Palustrine Scrub Shrub Wetland (19.2 percent), Developed (81.3 percent), and Deciduous Forest (89.4 percent). The highest combined accuracy for Bare Ground (88.5 percent) and Grass/Cultivated land cover (80.4 percent) was generated with concatenations of two different Standard Mode SAR images (*c*:S2A and *c*:S2D, respectively). Water was detected at 96.0 percent accuracy with c:PC_s. However, as Table 6 indicates, almost any merge technique was able to detect Water with high accuracy. It is also apparent from the above combined accuracy figures that land-cover types were not detected equally or at satisfactory accuracy levels for many applications.

It is assumed that, in an operational situation involving optical/SAR image merging, one initially would select a single optical image or image subset (i.e., bands 1 through *n*), a single SAR image, and a single SAR/optical image combination based on the optical data and SAR data accuracies. In this case, earlier work with the SAR data had found that the F2N image produced the highest SAR accuracy (Henderson *et al.*, 1998). Based on the findings of this research, the TM 1 through 5 and 7 data set (overall accuracy of 79.3 percent) and the *c*:F2N (overall accuracy of 82.4 percent) would be the preferred initial data sets. Table 6 provides the comparison of the combined accuracy of the TM data and this TM/SAR Concatenation for each land-cover category.

Observations

It is apparent that the combination of SAR/TM data using a single combination technique does not improve the accuracy of every land-cover category compared to using the optical data alone. The optimal combination varies by land cover and improvements range from quite modest to sizable.

SAR is sensitive to surface roughness/geometry and dielectric constant (moisture) differences. For example, SAR data should provide information about soil moisture and wetness conditions that would aid in the discrimination of forested wetlands from some upland forest. Sensitivity to geometry and surface roughness should assist in the separation of structures that might appear spectrally similar to beach or bare ground at optical wavelengths. Texture differences at microwave wavelengths could provide data to identify some cultivation, ground cover, or canopy conditions. With this in mind, it can be seen that, compared to TM data alone, SAR data contributed modestly to improved detection of Grass/Cultivated, Deciduous Forest, and Impervious land cover and substantively to Palustrine Forest, Developed, and Coniferous Forest land-cover detection.

Leckie (1998) has shown that the response of deciduous and coniferous forests on C-band imagery is complex and believes that it is necessary to map by species. Liao and Guo (1998) have shown C-band SAR to be sensitive to forest height and not density variation. We believe that the improvements added by SAR in this study are due in part to the differences in morphology, surface canopy, and stand height (the coniferous is generally higher) between these two vegetation groups, although the relative contribution of each factor is unknown. The contribution to Impervious and Developed land-cover detection is also due to the sensitivity of SAR to surface roughness and signal backscatter, in this case, the morphology and spatial densities of buildings and structures.

What is puzzling is the lack of improvement in the detection of Estuarine Emergent and Palustrine Emergent Wetland land cover. This may be due to the sparse vegetation density of these categories, the lack of foliage and leaf area at this time of year (April–May), and the relative water level. Kasischke *et al.* (1997) found that standing water caused forward scatter and lower radar backscatter from ERS imagery of herbaceous wetlands. However, they also stated that HH polarization should prove better than VV polarization and that C-band imagery should be preferred for detection of such wetlands. The observations of this study indicate that C-band HH polarized SAR imagery cannot detect herbaceous wetland at high accuracy levels in the conditions and season extant at the time of image acquisition. However, the f:$TM_{PC23457}$ + F2N did improve Estuarine Emergent detection by greater than 10 percent (68.1 percent for f:$TM_{PC23457}$ + F2N vs. 57.9 percent for TM).

Comparison of the combined accuracy figures for each land-cover category generated by classification of the TM data alone and those obtained with the best TM/SAR merge technique for that category indicates that merging TM and SAR data does

increase detection accuracy (albeit sometimes modestly) for all land-cover types but one—Palustrine Emergent wetland (Table 6). However, the preferred technique is land-cover type dependent. Presently, the reasons for this diversity in land-cover category/image merge combination improvement poses a conundrum from the perspective of research of radar backscatter response and data synthesis outcomes.

From an operational perspective, the variation in synthesis techniques suggests the use of a hierarchical classification (i.e., to employ a layered or stratified classifier in a series of steps usually proceeding from the general to more specific categories in a decision tree format) where one optical/SAR combination is selected as the primary data set for analysis. This procedure would be used, for example, when differences among image merge techniques were minor. Following the classification of the primary data set, other data set combinations would be created to mask out and improve the accuracy of a particular category (e.g., Estuarine Emergent Wetland). The masks might also include other ancillary data (e.g.. elevation data) to further enhance classification accuracy.

Summary

Four TM/SAR combination techniques were examined to determine their contribution in digitally classifying complex land cover mixtures in an urbanizing coastal environment. Among the findings were

- Concatenation of the SAR data to the TM data provided the highest overall accuracy of the 28 combinations tested.
- Image Addition and Image Weighting techniques might prove useful in other areas but were not effective in this instance.
- Image Fusion by principal component analysis was superior to other methods only in its ability to identify Estuarine Emergent Wetlands.
- Concatenation of SAR data with principal components of the TM data produced the highest accuracy for three land-cover types (Coniferous Forest, Impervious Surfaces, and Palustrine Scrub Shrub Wetland).
- Concatenation of a principal component of SAR data with TM data resulted in the highest accuracy for Developed, Deciduous Forest land cover, and Water.
- Merging TM with SAR data improved land-cover detection accuracy over that attained by TM data alone in all cases but one (Palustrine Emergent Wetland).
- Spatial resolution of SAR data appeared to be equal to if not more important than incident angle or polarization in achieving higher overall detection accuracy and for detection of cultural land-cover types. The results for natural cover types were mixed.
- The TM/F2N Radarsat Concatenation (*c*:F2N) produced the highest overall accuracy.
- For six of the eleven land-cover categories, the F2N image was the preferred SAR image in a merge technique and was a component in two others—but the specific merge technique varied.
- Concatenations of S2 Radarsat images generated the highest accuracy for the Bare Ground and Grass/Cultivated categories but one was an ascending pass and one was a descending pass. It is not known if this outcome is related to row direction and/or vegetation canopy cover or to simple serendipity, but the outcome is intriguing.
- The overall accuracy difference among all SAR/TM Image Concatenations varied by no more than 4.5 percent.
- Substitution of the SAR data for various TM principal components and limiting the total number of principal components in the fusion data sets showed little benefit. The greatest difference in overall accuracy was only 1.4 percent among the three variations tested.
- The overall accuracy of the ERS/TM Concatenation (*c*:ERS) performed slightly better than its Radarsat S1 Concatenation (*c*:S1) counterpart (as well as all other Radarsat Standard Mode Concatenations) largely due to ability to detect Coniferous Forest and two forest-related categories: Palustrine Forest and Palustrine Scrub Shrub. However, Radarsat Fine Mode Concatenations all performed better than the ERS data set.
- None of the C-band HH- and VV-polarized SAR/TM merged data sets could detect herbaceous or wooded wetlands at high combined accuracy levels (CA greater than 72.25 percent) in the environmental and seasonal conditions and at the categorical detail used in this study. Combined accuracies ranged from 7.0 percent to 68.1 percent.
- Simple Concatenation of the data sets proved as effective as any of the more robust image merge techniques. This was true for overall accuracy and each land-cover type except for Estuarine Emergent wetland detection.

This study used SAR imagery obtained during the spring (April-June) season. Wang *et al.* (1998) examined multi-date ERS-1 imagery of southern Ontario wetlands. They found that only multi-season data sets produced acceptable accuracies but that the best single date set was March. Baghdadi *et al.* (2001) classified six land-cover types in Ontario with multi-polarized C-band airborne SAR obtained on three dates. While cross-polarized data provided the best results, HH data was superior to the VV data. Morever, October was found to be the best time. Seasonal changes in land cover and wetlands of southern Hudson Bay, Ontario were also analyzed by Murphy *et al.* (2001) using Radarsat images. In this case, the best classification proved to be with May data, independent of incident angle.

The above studies, although focusing solely on SAR data of rural areas, are indicative of the mixed nature of SAR land-cover mapping results reported in the literature to date. The continuation of this mixed pattern is apparent in the variation in the urban/coastal SAR/TM findings reported here. Some findings agree with earlier work; others trend to be different. In this study, concatenation appears to be the most successful method of combining data sets of urban coastal environments. However, the results produced here should be tested in multiple environments (coastal, urban, and rural) and with imagery acquired at various seasons of the year. The potential of SAR/optical data set combinations for incorporation into hierarchical or layered classifications also merits consideration.

Acknowledgments

Funded in part by NOAA Contract NA67020344. The views expressed do not necessarily reflect those of NOAA, its subagencies, or the New York State Department of Health. Parts of this research were presented at the 25th Annual Conference of the Remote Sensing Society, 08–10 September 1999, Cardiff, Wales.

References

Baghdadi, N., M. Bernier, R. Gauthier, and I. Neeson, 2001. Evaluation of C-band SAR data for wetlands mapping, *International Journal of Remote Sensing*, 22 (1):71–88.

Chasan, Robert, 1998. *Urban Coastal Zone Land Cover Mapping with Combined Thematic Mapper/Radarsat Fine Mode Imagery: A Quantitative Approach*, MA thesis, University at Albany, Albany, New York, 131 p.

Chavez, P.S., Jr., S.C. Sides, and J.A. Anderson, 1991. Comparison of three different methods to merge multiresolution and multispectral data: Landsat TM and SPOT data, *Photogrammetric Engineering & Remote Sensing*, 53(7):295–303.

Cracknell, A.P., 1999. Remote sensing techniques in estuaries and coastal zones—An update, *International Journal of Remote Sensing*, 19(3):485–496.

Dobson, M.C., F.T. Ulaby, and L.E. Pierce, 1995a. Land-cover classification and estimation of terrain attributes using synthetic aperture radar. *Remote Sensing of Environment*, 51(1):199–214.

Dobson, J.E., E.A. Bright, R.L. Ferguson, D.W. Field, L.L. Wood, K.D. Haddad, H. Iredale III, J.R. Jensen, V.V. Klemas, R.J. Orth, and J.P. Thomas, 1995b. *NOAA Coastal Change Analysis Program (C-CAP): Guidance for Regional Implementation*, NOAA Technical Report NMFS 123, U.S. Department of Commerce, Seattle Washington, 92 p.

Dobson, M.C., L.E. Pierce, and F.T. Ulaby, 1996. Knowledge-based land-cover classification using ERS-1/JERS-1 SAR composites, *IEEE Transactions of Geoscience and Remote Sensing*, 34(1):83–99.

Dong, Y., B. Forster, and C. Ticehurst, 1997. Radar backscatter analysis for urban environments, *International Journal of Remote Sensing*, 18(6):1351–1364.

Durand, J.M., B.J. Gimonett, and J.R. Derbos, 1987. SAR data filtering for classification, *IEEE Transactions on Geoscience and Remote Sensing*, GE-25(5):629–637.

Heaton, Brian P., 1998. *Fusion of Multispectral Multisensor Imagery to Improve Wetland Detection Ability*, MA thesis, University at Albany, Albany, New York, 85 p.

Henderson, F.M., and Z.G. Xia, 1998. Radar application in urban analysis, settlement detection, and population analysis, *Principles and Applications of Imaging Radar* (F.M. Henderson and A.J. Lewis, editors), John Wiley and Sons, New York, N.Y., pp. 733–768.

Henderson, F.M., R. Chasan, J. Portolese, and T.F. Hart, Jr., 1998. Contribution of SAR data and image concatenation in reducing optical sensor-derived urban land cover confusion, *Proceedings of the Second International Workshop on Retrieval of Bio- and Geo-Physical Parameters from SAR Data for Land Applications*, 21–23 October, ESTEC, Noordwijk, The Netherlands, pp. 51–58.

Henderson, F.M., T. Hart, Jr., B. Heaton, and J. Portolese, 1999. Mapping coastal ecosystems over a steep development gradient using C-CAP protocols, *International Journal of Remote Sensing*, 60 (3):727–744.

Jensen, J.R., D.J. Cowan, J.D. Althausen, S. Narumalani, and O. Weatherbee, 1993. An evaluation of the Coastwatch Change Detection Protocol in South Carolina, *Photogrammetric Engineering & Remote Sensing*, 59(6):1039–1046.

Kalkhan, M.A., R.M. Reich, and R.L. Czaplewski, 1997. Variance estimates and confidence intervals for the Kappa measure of classification accuracy, *Canadian Journal of Remote Sensing*, 23(3):210–216.

Kasischke, E.S., J.M. Melack, and M.C. Dobson, 1997. The use of imaging radars for ecological applications—A review, *Remote Sensing of Environment*, 59(1):141–156.

Kershaw, C.D., and R.M. Fuller, 1992. Statistical problems in the discrimination of land cover from satellite images: A case study in lowland Britain, *International Journal of Remote Sensing*, 13(16):3085–3104.

Leckie, D.G., 1998. Forestry applications using imaging radar, *Principles and Applications of Imaging Radar* (F.M. Henderson and A.J. Lewis, editors), John Wiley and Sons, Inc., New York, N.Y., pp. 435–510.

Lee, J.S., I. Jurkevich, P. Dewaele, P. Wambacq, and A. Oosterlinck, 1994. Speckle filtering of synthetic aperture radar images: A review, *Remote Sensing Reviews*, 8(4):313–340.

Lewis, A.J., D.H. Braud, Jr., and B.M. Territo, 1995. *Merging Landsat TM Satellite Imagery and Airborne Synthetic Aperture Radar to Facilitate Coastline Delineation*, Louisiana State University, Baton Rouge, Louisiana, unpublished, 60 p.

Liao, J., and H. Guo, 1998. Multifrequency and multipolarization radar data for estimation of forest volume over the Zhaoqing area of southern China, *Canadian Journal of Remote Sensing*, 24(3):240–245.

Lozano-Garcia, D.F., and R. Hoffer, 1993. Synergistic effects of combined Landsat-TM and SIR-B data for forest resources assessment, *International Journal of Remote Sensing*, 14(14):267–269.

Mitsch, W.J., and J.G. Gosselink, 1993. Wetlands, *Second Edition*, Van Nostrand Reinhold, New York, N.Y., 721 p.

Monserud, R.A., and R. Leemans, 1992. Comparing global vegetation maps with the Kappa statistic, *Ecological Modeling*, 62(4):275–293.

Murphy, M.A., I.P Martini, and R. Protz, 2001. Seasonal changes in subarctic wetlands and river ice breakup detectable on RADARSAT images, southern Hudson Bay lowland, Ontario, Canada, *Canadian Journal of Remote Sensing*, 27(2):143–158.

Pohl, C., and J.L. VanGenderen, 1998. Multisensor image fusion in remote sensing: concepts, methods and applications, *International Journal of Remote Sensing*, 19(5):823–854.

Schmullis, C.C., and D.L. Evans, 1997. Synthetic aperture radar (SAR) frequency and polarization requirements for applications in ecology, geology, hydrology, and oceanography: A tabular status quo after SIR-C/X-SAR, *International Journal of Remote Sensing*, 18(13):2713–2722.

Sharma, K.M.S., and A. Sarkar, 1998. A modified contextual classification technique for remote sensing data, *Photogrammetric Engineering & Remote Sensing*, 64(4):273–280.

Taket, N.D., S.M. Howarth, and R.E. Burge, 1991. A model for the imaging of urban areas by synthetic aperture radar, *IEEE Transactions on Geoscience and Remote Sensing*, 29(3):432–443.

Toll, D., 1985. Analysis of Digital Landsat MSS and SEASAT SAR data for use in discrimination land cover at the urban fringe of Denver, Colorado, *International Journal of Remote Sensing*, 6(7): 1209–1229.

Wang, J., J. Shang, B. Brisco, and R.J. Brown, 1998. Evaluation of multidate ERS-1 and multispectral Landsat imagery for wetland detection in southern Ontario, *Canadian Journal of Remote Sensing*, 24(1):60-68.

(Received 22 June 2000; revised and accepted 19 December 2001; revised 26 December 2001)